JOURNAL OF SOLID STATE CHEMISTRY **141,** 177–185 (1998)
ARTICLE NO. SC987942

Crystal Structures and Crystal Chemistry of $AgXPO_4$ (X = Be, Zn)

Robert Hammond, Jacques Barbier,[1] and Cyril Gallardo

Department of Chemistry, McMaster University, Hamilton, Ontario L8S 4M1, Canada

Received February 17, 1998; in revised form May 18, 1998; accepted June 24, 1998

The crystal structures of the tetrahedral framework compounds $AgBePO_4$, low-T α-$AgZnPO_4$, and high-T β-$AgZnPO_4$ have been determined by X-ray diffraction using single crystals grown from a silver molybdate flux. $AgBePO_4$ ($a = 8.213(3)$ Å, $b = 7.884(3)$ Å, $c = 14.424(7)$ Å, $\beta = 90.20(3)^\circ$, $P2_1/n$, $Z = 12$, $wR(F^2) = 0.091$) and β-$AgZnPO_4$ ($a = 8.695(2)$ Å, $b = 8.107(1)$ Å, $c = 15.375(2)$ Å, $\beta = 90.38(1)^\circ$, $P2_1/n$, $Z = 12$, $wR(F^2) = 0.074$) are isostructural and adopt a beryllonite-type framework with a mixed UDUDUD + UUDDUD topology. α-$AgZnPO_4$ ($a = 10.218(2)$ Å, $c = 7.948(1)$ Å, $P6_3$, $Z = 8$, $wR(F^2) = 0.054$) crystallizes with a structure similar to those of high-T $NaCoPO_4$ and $KZnPO_4$, with a mixed UDUDUD + UUUDDD framework topology. The phase transformation occurring at 670°C in $AgZnPO_4$ and the absence thereof in $AgBePO_4$ are discussed in terms of the bonding environments around the Ag^+ cations in their crystal structures.

INTRODUCTION

Compounds belonging to the large structural family of tridymite derivatives (1) have been of continuing interest due to their structural properties, such as their open-framework architecture and their polymorphism in particular (2–8), as well as their physical properties, including their ferroic properties or their potential as hosts for fluorescent materials (9–12). The monophosphate compounds $A^{I}X^{II}PO_4$ (with X^{II} = Be, Zn and $A^{I} = Na^+ \rightarrow Cs^+$, Tl^+, Ag^+ and NH_4^+) are known to belong to that structural family, their structures consisting of a [$BePO_4$] or [$ZnPO_4$] tetrahedral framework with cavities filled with the monovalent cations. Partial structural data (e.g., cell dimensions from powder X-ray diffraction data) are available for most $A^{I}X^{II}PO_4$ compounds (13, 14) and full structure determinations have been carried out for the following members of the series: the beryllonite mineral $NaBePO_4$ (15), $KBePO_4$ and $CsBePO_4$ (16), $TlBePO_4$ (17), $NaZnPO_4$ (18), $KZnPO_4$ (19), $RbZnPO_4$ (20), and $CsZnPO_4$ (21). Several of these compounds, including $NaZnPO_4$, $KZnPO_4$, and $CsZnPO_4$, are known to be polymorphic but, except for the cesium compound, the structure of only one polymorph has been determined. In the case of the silver compounds, no structural information at all is available for $AgBePO_4$ and only unit cell dimensions have been determined for $AgZnPO_4$ (13, 22). The latter has also been observed to undergo an unusual phase transformation at 666°C from a low-temperature hexagonal phase to a high-temperature monoclinic phase (22) and, on the basis of X-ray powder data, the monoclinic phase has been described as beryllonite-like and the hexagonal phase as nepheline-like (for the latter, in spite of some significant discrepancies between the observed and calculated X-ray intensities). As part of an ongoing study of the crystal chemistry and polymorphism of tetrahedral framework compounds which are tridymite derivatives [e.g., (4) and (6)], the crystal structures of α-$AgZnPO_4$ (low T), β-$AgZnPO_4$ (high T), and $AgBePO_4$ have been determined by single-crystal X-ray diffraction. These structures are described here together with a discussion of the polymorphism in $AgZnPO_4$.

EXPERIMENTAL

The $AgBePO_4$ and $AgZnPO_4$ compounds were initially synthesized in polycrystalline form from stoichiometric mixtures of $AgNO_3$, BeO, ZnO, and $NH_4H_2PO_4$ powders (all reagent grade), pressed into pellets of 0.4 g each. The progress of the solid-state reactions was followed by powder X-ray diffraction with a Guinier–Hägg camera using Cu$K\alpha_1$ radiation and silicon as an internal standard. The line positions and intensities on the powder X-ray films were measured with a digital LS20 film scanner (KEJ Instruments, Täby, Sweden). After firing at 600°C for 1 day with one intermediate remixing, the $AgBePO_4$ sample was found to be single phase and its powder pattern could be entirely indexed on the following beryllonite-type monoclinic unit cell: $a = 8.219(1)$ Å, $b = 7.885(2)$ Å, $c = 14.436(2)$ Å, and $\beta = 90.45(1)^\circ$, with extinctions consistent with the $P2_1/n$ space group. In the case of $AgZnPO_4$, the low-temperature α-phase was synthesized first by firing the pellet between 450

[1] To whom correspondence should be addressed. E-mail: barbier@mcmaster.ca.

0022-4596/98 $25.00

and 550°C for 3 days with one intermediate remixing. Its X-ray powder pattern was completely indexed on the following hexagonal cell: $a = 10.255(4)$ Å and $c = 7.973(5)$ Å, with extinctions consistent with the $P6_3$ space group. No diffraction line corresponding to the $2 \times c$ superstructure reported previously (20) could be detected. The high-temperature β-phase was obtained by heating the α-phase to 750°C for 1 day, followed by quenching in air. Its X-ray powder pattern was indexed on a beryllonite-type monoclinic unit cell with the following parameters: $a = 8.740(1)$ Å, $b = 8.135(1)$ Å, $c = 15.447(2)$ Å, $\beta = 90.35(1)°$, $P2_1/n$ space group. These parameters are all slightly larger than those of the $AgBePO_4$ phase as expected from the difference between the Zn–O and Be–O bond distances.

The phase transformation in $AgZnPO_4$ was also confirmed by DTA and DSC measurements. Upon heating the α-phase powder from room temperature at a rate of 10°C/min, the $\alpha \rightarrow \beta$ transformation was indicated by an endothermic peak at 671°C, followed by melting at 784°C. These temperatures are in good agreement with those reported by Andratschke (22) but differ from the earlier results of Quarton *et al.* (23), who did not identify any transition. Although the reverse $\beta \rightarrow \alpha$ transformation could not be observed during the cooling cycles of the DTA or DSC experiments (due to the sluggishness of the reconstructive transformation; cf. later), the β-phase could be completely transformed back into the α-phase after heating at 400°C for 24 h. Similar experiments were also carried out for the $AgBePO_4$ compound but, in this case, no evidence of a polymorphic transformation was found during heating of the sample up to the melting point of 1160°C in a DTA apparatus.

Single crystals of the $AgBePO_4$, α-$AgZnPO_4$, and β-$AgZnPO_4$ phases suitable for X-ray diffraction were grown from a silver molybdate flux. In each case, a prereacted powder sample was dissolved in the $Ag_2Mo_2O_7$ flux contained in a platinum crucible, the solution was homogenized at high temperature for several days, and the temperature was then decreased slowly over a range of 75°C or more, followed by quenching in air. The specific growth conditions used for the three different phases are listed in Table 1. Note that the temperature ranges used for the growth of the low-T (α) and high-T (β) forms of $AgZnPO_4$ remained correspondingly below and above the transition temperature of 670°C. The much larger nutrient/flux ratio used for the growth of the β-$AgZnPO_4$ crystals was required due to the high solubility of the nutrient in the flux at higher temperature. In all cases, the crystals were separated from the flux by dissolving the latter in hot aqueous ammonium hydroxide solutions. It was found later on that the $AgZnPO_4$ compound also had a significant solubility in concentrated NH_4OH solutions and this may account for the silver deficiency found in the β-$AgZnPO_4$ crystals (cf. later). Good-quality crystals, free of twinning and defects, were selected for the collection of X-ray data by examination with an optical microsocope under polarized light.

TABLE 1
Flux Growth Conditions for $AgBePO_4$, α-$AgZnPO_4$, and β-$AgZnPO_4$ Single Crystals

	$AgBePO_4$	α-$AgZnPO_4$	β-$AgZnPO_4$
$Ag_2Mo_2O_7$ flux (g)	7.01	11.84	2.28
Nutrient (g)	0.50	0.84	4.71
Soak temperature (°C)	700	500	750
Soak time (days)	3	3	3
Cooling rate (°C/hr)	3.0	3.0	2.4
Final temperature (°C)	400	350	675
Crystal composition[a]	$AgBePO_4$	$Ag_{0.98}Zn_{0.99}P_{1.01}O_4$	$Ag_{0.79}Zn_{1.00}P_{1.00}O_4$

[a] From microprobe analyses using the $AgBePO_4$ crystals as standard. The Ag^+-cation deficiency in the β-$AgZnPO_4$ crystals is assumed to be compensated by NH_4^+ ions (see text).

To confirm their chemical compositions, a few crystals of each of the $AgBePO_4$ and $AgZnPO_4$ phases were analyzed by an electron microprobe. Because the initial structure determination of the $AgBePO_4$ compound did not suggest any deviation from the nominal composition (i.e., the occupancies of the Ag positions did not deviate from unity and the U_{eq} displacement parameters all had reasonable values; see Table 3), the $AgBePO_4$ crystals were used as calibration standards for the electron microprobe. The Ag, Zn, and P contents of the α- and β-$AgZnPO_4$ crystals were then determined by analyzing three different crystals for each phase, yielding the averaged chemical compositions listed in Table 1. These analyses show clearly that, whereas the composition of the α-$AgZnPO_4$ crystals does not significantly deviate from the nominal composition, the β-$AgZnPO_4$ crystals are strongly deficient in silver with a composition of $Ag_{0.79}Zn_{1.00}P_{1.00}O_4$. Their low silver content is in good agreement with the Ag-site occupancies refined during the X-ray structure determination (yielding an average occupancy of 82% for the three Ag sites of the β-$AgZnPO_4$ structure; see later). The measured Ag_2O (37.2 wt%), ZnO (32.8 wt%), and P_2O_5 (28.8 wt%) contents of the β-$AgZnPO_4$ crystals are also all in good agreement with the corresponding values of 37.8, 32.4, and 28.2 wt% corresponding to the final $Ag_{0.82}(NH_4)_{0.18}ZnPO_4$ composition used in the X-ray work (see later).

The details of the data collections and structure refinements for $AgBePO_4$, α-$AgZnPO_4$, and β-$AgZnPO_4$ are listed in Table 2. In all cases, the raw intensity data were first corrected for absorption using the empirical ψ-scan method and the structures were then solved by a combination of direct methods and Fourier syntheses, followed by fully anisotropic refinements using the SHELXTL and SHELXL93 software (24, 25). The final atomic coordinates, isotropic displacement parameters, and anisotropic displacement parameters are listed in Tables 3–5. No

TABLE 2
Data Collections and Structure Refinements for $AgBePO_4$, β-$AgZnPO_4$ and α-$AgZnPO_4$

Structure	$AgBePO_4$	β-$AgZnPO_4$	α-$AgZnPO_4$
Chemical composition[a]	$AgBePO_4$	$Ag_{0.82}(NH_4)_{0.18}ZnPO_4$	$AgZnPO_4$
Space group	$P2_1/n$	$P2_1/n$	$P6_3$
Z	12	12	8
a (Å)	8.213(3)	8.695(2)	10.218(2)
b (Å)	7.884(3)	8.107(1)	
c (Å)	14.424(7)	15.375(2)	7.948(1)
α (deg)	90	90	90
β (deg)	90.20(3)	90.38(1)	90
γ (deg)	90	90	120
V (Å^3)	934.0(9)	1083.7(5)	718.6(3)
D_x (Mg m^{-3})	4.52	4.64	4.96
Radiation	Ag$K\alpha$	Ag$K\alpha$	Ag$K\alpha$
Absorption coefficient (mm^{-1})	3.59	6.29	6.52
Temperature	Room temperature	Room temperature	Room temperature
Description	Irregular prism	Irregular prism	Hexagonal prism
Size (mm)	$0.11 \times 0.13 \times 0.13$	$0.15 \times 0.22 \times 0.33$	$0.15 \times 0.16 \times 0.28$
Diffractometer type	Siemens R3m/V	Siemens R3m/V	Siemens R3m/V
Collection method	2θ–θ	2θ–θ	2θ–θ
2θ max (deg)	65.2	60.2	60.2
h_{min}, h_{max}	0, 15	−1, 15	−15, 0
k_{min}, k_{max}	0, 15	−1, 14	0, 18
l_{min}, l_{max}	−27, 27	−27, 27	−14, 14
Observed reflections	7608	8528	2882
Absorption correction	ψ-scan	ψ-scan	ψ-scan
T_{min}, T_{max}	0.501, 0.554	0.618, 0.982	0.340, 0.515
Independent reflections	6924	6463	2882
R_{int}	0.030	0.031	n/a
Parameters refined	190	203	92
Reflections used	6921	6463	2882
Reflections with $F_o > 4\sigma(F_o)$	3623	4706	2638
Weighting scheme		$[\sigma^2(F_o^2) + (wP)^2]^{-1}$ with $P = (\max(F_o^2, 0) + 2F_c^2)/3$	
Weighting parameter (w)	0.032	0.040	0.027
Extinction correction		$(1 + 0.001(c)\,F_c^2 l^3/\sin^2\theta)^{-1/4}$	
Extinction parameter c	n/a	0.0487(8)	0.0246(9)
Atomic scattering factors		Neutral atoms from SHELXL software	
$wR(F^2)$ (all)	0.091	0.074	0.054
$R(F)$ ($F_o > 4\sigma(F_o)$)	0.044	0.049	0.024
S	0.845	0.931	1.017
$(\Delta/\sigma)_{max}$	0.001	0.012	−0.035
$(\Delta\rho)_{min}$ (e Å^{-3})	−2.5	−1.7	−1.0
$(\Delta\rho)_{max}$ (e Å^{-3})	1.4	1.5	1.4

[a] Chemical composition from electron microprobe analysis (see text).

particular difficulty was encountered during the structure determinations of $AgBePO_4$ and α-$AgZnPO_4$ and the refinement of Ag-site occupancies did not indicate any significant deviation from the nominal compositions in either case. In the final cycles of the refinement of the α-$AgZnPO_4$ structure, the strongly anisotropic displacement of the O(6) atom was resolved by moving it off the threefold axis, thereby eliminating an unfavorable Zn–O(6)–P bond angle of 180° and achieving better Zn–O(6) and P–O(6) bond lengths (cf. Tables 5 and 8). Similar oxygen-site splittings have been used in the $P6_3$ refinements of hexagonal kalsilite ($KAlSiO_4$) (26), nepheline [$(Na_{0.75}K_{0.25})AlSiO_4$] (27), and $(Na_{0.75}K_{0.25})AlGeO_4$ (28). In the case of β-$AgZnPO_4$, the initial refinement based on the ideal stoichiometry did not converge properly (yielding a residual $wR(F^2) = 0.176$) and the electron density difference map contained large holes (approximately −6.5 e Å^{-3}) near all Ag positions. The subsequent refinement of the Ag-site occupancies quickly revealed a strong Ag deficiency on all three sites (between 79 and 88%; cf. Table 4), which agreed very well with the electron microprobe analysis (vide supra). To maintain electroneutrality, it was then assumed that the Ag^+ deficiency

TABLE 3

Atomic Coordinates ($\times 10^5$ for Ag and P, $\times 10^4$ for Be and O) and Equivalent Isotropic Displacement Parameters (in Å^2, $\times 10^4$) for $AgBePO_4$

Atom	x	y	z	U_{eq}
Ag(1)	25005(4)	1193(4)	24868(2)	157(1)
Ag(2)	72343(4)	48046(4)	8613(2)	182(1)
Ag(3)	78699(4)	1441(4)	6469(2)	163(1)
P(1)	58152(11)	29167(11)	26205(6)	67(1)
P(2)	10561(11)	29595(11)	8252(6)	66(1)
P(3)	7024(11)	29382(11)	40988(6)	63(1)
Be(1)	9208(6)	1742(6)	2416(3)	85(7)
Be(2)	4044(6)	1730(6)	4193(3)	77(7)
Be(3)	4344(6)	1705(6)	916(3)	97(8)
O(1)	4470(3)	2683(3)	1895(2)	104(4)
O(2)	627(3)	2743(3)	1849(2)	113(4)
O(3)	2501(3)	2819(3)	3811(2)	108(4)
O(4)	7466(3)	2551(4)	2177(2)	133(5)
O(5)	9577(3)	2527(3)	213(2)	102(4)
O(6)	5534(3)	2546(3)	126(2)	106(4)
O(7)	5530(3)	1756(3)	3461(2)	99(4)
O(8)	2459(3)	1768(3)	568(2)	98(4)
O(9)	9671(3)	1727(3)	3508(2)	99(4)
O(10)	5731(3)	4775(3)	2955(2)	133(4)
O(11)	1607(3)	4787(3)	664(2)	103(4)
O(12)	99(3)	4745(3)	3933(2)	106(4)

Anisotropic displacement parameters (in Å^2, $\times 10^4$) for $AgBePO_4$

Atom	U_{11}	U_{22}	U_{33}	U_{23}	U_{13}	U_{12}
Ag(1)	155(1)	155(1)	161(1)	6(1)	1(1)	5(1)
Ag(2)	220(1)	146(1)	179(1)	− 32(1)	92(1)	− 14(1)
Ag(3)	199(1)	155(1)	134(1)	− 6(1)	− 57(1)	− 21(1)
P(1)	69(3)	71(3)	59(3)	4(3)	5(3)	4(3)
P(2)	70(4)	66(3)	62(3)	3(3)	− 1(3)	0(3)
P(3)	64(3)	66(3)	59(3)	− 1(3)	0(3)	4(3)
Be(1)	70(2)	100(2)	80(2)	20(14)	2(15)	27(14)
Be(2)	90(2)	70(2)	70(2)	4(13)	− 5(15)	− 5(14)
Be(3)	70(2)	100(2)	120(2)	− 22(15)	10(2)	3(14)
O(1)	66(10)	153(12)	94(10)	− 40(8)	6(8)	10(9)
O(2)	92(10)	163(12)	85(10)	4(9)	23(8)	− 43(9)
O(3)	78(10)	129(11)	118(10)	26(9)	− 2(8)	16(9)
O(4)	98(10)	203(13)	98(10)	36(9)	35(9)	31(10)
O(5)	66(9)	127(11)	114(11)	32(8)	− 6(8)	− 18(8)
O(6)	123(11)	113(10)	82(10)	− 8(8)	5(8)	− 29(9)
O(7)	110(10)	96(10)	90(10)	33(8)	28(8)	33(8)
O(8)	97(10)	76(10)	120(10)	− 44(8)	− 22(8)	24(8)
O(9)	133(11)	81(9)	83(10)	− 6(8)	− 22(8)	− 47(9)
O(10)	219(12)	76(9)	103(10)	7(9)	− 39(9)	1(10)
O(11)	112(10)	67(8)	131(10)	9(8)	41(8)	3(9)
O(12)	115(10)	62(8)	142(10)	− 15(8)	− 11(8)	− 8(8)

TABLE 4

Atomic Coordinates ($\times 10^5$ for Ag, Zn, and P $\times 10^4$ for O) and Equivalent Isotropic Displacement Parameters (in Å^2, $\times 10^4$) for β-$AgZnPO_4$

Atom	x	y	z	U_{eq}	Occupancy[a]
Ag(1)	24949(4)	− 143(6)	24644(3)	292(1)	0.807(2)
Ag(2)	73046(4)	47859(4)	8978(2)	245(1)	0.790(2)
Ag(3)	78378(3)	935(4)	6414(2)	244(1)	0.882(2)
P(1)	92385(6)	18240(7)	23558(3)	116(1)	
P(2)	40061(6)	18228(7)	42088(3)	117(1)	
P(3)	43999(6)	17981(7)	9104(3)	119(1)	
Zn(1)	58327(3)	28903(3)	26371(2)	148(1)	
Zn(2)	10624(3)	29328(3)	8156(2)	148(1)	
Zn(3)	6628(3)	28791(3)	40896(2)	146(1)	
O(1)	4207(2)	2727(2)	17721(1)	206(3)	
O(2)	647(2)	2805(3)	2050(1)	232(4)	
O(3)	2782(2)	2769(2)	3692(1)	205(3)	
O(4)	7782(2)	2705(3)	2067(1)	277(4)	
O(5)	9423(2)	2225(2)	40(1)	229(4)	
O(6)	5464(2)	2749(2)	297(1)	221(3)	
O(7)	5436(2)	1557(2)	3651(1)	185(3)	
O(8)	2807(2)	1588(2)	494(1)	205(3)	
O(9)	9306(2)	1607(2)	3342(1)	179(3)	
O(10)	5683(3)	5135(2)	3084(1)	321(5)	
O(11)	1665(2)	5154(2)	529(1)	230(4)	
O(12)	− 102(2)	5107(2)	3909(1)	237(4)	

Anisotropic displacement parameters (in Å^2, $\times 10^4$) for β-$AgZnPO_4$

Atom	U_{11}	U_{22}	U_{33}	U_{23}	U_{13}	U_{12}
Ag(1)	261(2)	295(2)	319(1)	− 2(1)	− 25(1)	37(2)
Ag(2)	266(2)	247(1)	222(1)	− 58(1)	82(1)	− 42(1)
Ag(3)	228(1)	294(1)	209(1)	− 42(1)	− 50(1)	− 60(1)
P(1)	110(2)	138(2)	99(2)	2(2)	− 10(2)	− 5(2)
P(2)	99(2)	142(2)	109(2)	4(2)	0(2)	6(2)
P(3)	102(2)	142(2)	112(2)	− 12(2)	− 9(2)	− 2(2)
Zn(1)	135(1)	181(1)	128(1)	3(1)	− 2(1)	− 3(1)
Zn(2)	131(1)	180(1)	132(1)	− 11(1)	− 1(1)	0(1)
Zn(3)	127(1)	177(1)	134(1)	− 14(1)	− 9(1)	6(1)
O(1)	144(7)	323(9)	149(6)	− 91(6)	− 24(5)	26(7)
O(2)	161(7)	392(10)	142(6)	19(7)	4(5)	− 111(7)
O(3)	117(6)	323(9)	174(7)	72(6)	− 3(5)	48(7)
O(4)	145(7)	434(11)	253(8)	141(8)	36(6)	90(8)
O(5)	212(8)	259(8)	214(7)	97(6)	− 98(6)	− 85(7)
O(6)	277(9)	249(8)	139(6)	− 19(6)	30(6)	− 114(7)
O(7)	141(7)	219(8)	197(7)	64(6)	55(6)	45(6)
O(8)	125(7)	261(8)	227(8)	− 97(6)	− 64(6)	45(6)
O(9)	209(8)	209(7)	118(6)	5(5)	− 14(5)	− 74(6)
O(10)	650(2)	154(7)	163(7)	28(6)	− 43(9)	− 26(9)
O(11)	238(9)	150(7)	303(9)	0(6)	118(7)	31(6)
O(12)	210(8)	146(7)	355(10)	− 24(6)	− 103(7)	− 1(6)

[a] The cation deficiency on the Ag(1–3) sites is compensated by the introduction of NH_4^+ ions (see text).

was compensated by the introduction of NH_4^+ cations and the mixed Ag^+/NH_4^+ site occupancies converged rapidly to the values listed in Table 4. This assumption is based on the possibility of a partial NH_4^+/Ag^+ ion exchange taking place during the dissolution of the $Ag_2Mo_2O_7$ flux in the hot NH_4OH aqueous solution in which the crystals themselves have later been found to be somewhat soluble. It should be noted, however, that there was no direct evidence for the presence of NH_4^+ ions in the β-$AgZnPO_4$ crystals and that the refinement was rather insensitive to the introduction of

TABLE 5
Atomic Coordinates ($\times 10^5$ for Ag, Zn, and P $\times 10^4$ for O) and Equivalent Isotropic Displacement Parameters (in Å^2, $\times 10^4$) for α-$AgZnPO_4$

Atom	x	y	z	U_{eq}
Ag(1)	0	0	47630(4)	256(1)
Ag(2)	95930(3)	47882(3)	47734(3)	237(1)
Zn(1)	33333	66667	66216(6)	114(1)
Zn(2)	33088(3)	18460(3)	79872(4)	123(1)
P(1)	33333	66667	23752(13)	109(2)
P(2)	32824(7)	18841(7)	19977(8)	92(1)
O(1)	3107(2)	2895(2)	3301(2)	150(3)
O(2)	1883(2)	305(2)	2032(3)	165(3)
O(3)	4696(2)	1771(2)	2388(2)	150(3)
O(4)	4874(2)	6976(2)	1709(2)	188(3)
O(5)	3407(2)	2594(2)	263(2)	164(3)
O(6)[a]	3111(8)	6621(16)	258(5)	169(11)

Anisotropic displacement parameters (in Å^2, $\times 10^4$) for α-$AgZnPO_4$[b]

Atom	U_{11}	U_{22}	U_{33}	U_{23}	U_{13}	U_{12}
Ag(1)	283(1)	283(1)	202(2)	0	0	141(1)
Ag(2)	297(1)	282(1)	232(1)	42(1)	44(1)	221(1)
Zn(1)	106(1)	106(1)	132(2)	0	0	53(1)
Zn(2)	118(1)	120(1)	137(1)	− 1(1)	0(1)	64(1)
P(1)	108(2)	108(2)	111(4)	0	0	54(1)
P(2)	85(2)	82(2)	112(2)	8(2)	4(2)	44(2)
O(1)	166(7)	193(7)	132(6)	− 48(5)	− 28(5)	120(6)
O(2)	110(6)	96(6)	261(7)	29(6)	− 23(6)	30(5)
O(3)	100(6)	140(7)	219(7)	46(6)	14(5)	68(6)
O(4)	113(7)	218(8)	242(8)	− 81(7)	− 21(6)	88(6)
O(5)	272(9)	147(7)	96(6)	21(5)	10(5)	122(7)

[a] Oxygen position split around the threefold axis with 1/3 occupancy.
[b] An isotropic displacement parameter was retained for the split O(6) atom in the final refinement.

TABLE 6
Bond Lengths (l, Å), Bond Valences (s) and Selected Bond Angles (Deg) in $AgBePO_4$[a]

	l	s		
			P(1)–O(10)	1.544(3)
			P(2)–O(2)	1.528(3)
Ag(1)–O(2)#1	2.605(3)	0.115	P(2)–O(11)	1.529(3)
Ag(1)–O(3)#1	2.606(3)	0.115	P(2)–O(8)	1.533(3)
Ag(1)–O(1)#1	2.668(3)	0.097	P(2)–O(5)#2	1.538(3)
Ag(1)–O(1)	2.728(3)	0.083		
Ag(1)–O(2)	2.735(3)	0.081	P(3)–O(12)	1.527(3)
Ag(1)–O(10)#1	2.740(3)	0.080	P(3)–O(9)#2	1.533(3)
Ag(1)–O(11)#1	2.777(3)	0.072	P(3)–O(6)#10	1.536(3)
Ag(1)–O(3)	2.859(3)	0.058	P(3)–O(3)	1.539(3)
Ag(1)–O(12)#1	2.863(3)	0.057		
Ag(1)–O(9)#2	3.033(3)	0.036	Be(1)–O(4)	1.603(5)
Ag(1)–O(8)	3.058(3)	0.034	Be(1)–O(9)	1.620(5)
Ag(1)–O(7)	3.132(3)	0.028	Be(1)–O(2)#11	1.630(5)
	$\sum s$	0.86	Be(1)–O(10)#7	1.640(5)
Ag(2)–O(9)#3	2.363(3)	0.221	Be(2)–O(7)	1.616(5)
Ag(2)–O(11)#4	2.421(2)	0.189	Be(2)–O(3)	1.626(5)
Ag(2)–O(6)	2.497(3)	0.154	Be(2)–O(11)#1	1.636(5)
Ag(2)–O(7)#3	2.584(3)	0.122	Be(2)–O(5)#10	1.642(5)
Ag(2)–O(4)	2.607(3)	0.114		
Ag(2)–O(5)	2.795(3)	0.069	Be(3)–O(1)	1.611(5)
[Ag(2)–O(1)	3.193(3)	0.023][b]	Be(3)–O(12)#1	1.626(5)
[Ag(2)–O(10)	3.266(3)	0.019]	Be(3)–O(8)	1.627(5)
	$\sum s$	0.87	Be(3)–O(6)	1.644(5)
Ag(3)–O(8)#6	2.327(2)	0.244		
Ag(3)–O(10)#7	2.336(3)	0.238	P(1)–O(1)–Be(3)	134.5(2)
Ag(3)–O(5)	2.427(3)	0.186	P(2)–O(2)–Be(1)#2	134.9(3)
Ag(3)–O(12)#1	2.534(3)	0.139	P(3)–O(3)–Be(2)	133.5(2)
Ag(3)–O(6)	2.797(3)	0.068	P(1)–O(4)–Be(1)	141.1(2)
Ag(3)–O(4)	2.930(3)	0.048	P(2)#11–O(5)–Be(2)#5	130.0(2)
[Ag(3)–O(3)#5	3.112(3)	0.029]	P(3)#5–O(6)–Be(3)	128.6(2)
[Ag(3)–O(5)#8	3.223(3)	0.022]	P(1)–O(7)–Be(2)	129.8(2)
	$\sum s$	0.92	P(2)–O(8)–Be(3)	131.3(2)
			P(3)#11–O(9)–Be(1)	131.6(2)
P(1)–O(4)	1.529(3)		P(1)–O(10)–Be(1)#3	142.5(2)
P(1)–O(1)	1.531(3)		P(2)–O(11)–Be(2)#9	140.0(2)
P(1)–O(7)	1.538(3)		P(3)–O(12)–Be(3)#9	140.8(2)

[a] Symmetry transformations used to generate equivalent atoms: #1, $-x+\frac{1}{2},y-\frac{1}{2},-z+\frac{1}{2}$; #2, $x-1,y,z$; #3, $-x+\frac{3}{2},y+\frac{1}{2},-z+\frac{1}{2}$; #4, $-x+1,-y+1,-z$; #5, $x+\frac{1}{2},-y+\frac{1}{2},z-\frac{1}{2}$; #6, $-x+1,-y,-z$; #7, $-x+\frac{3}{2},y-\frac{1}{2},-z+\frac{1}{2}$; #8, $-x+2,-y,-z$; #9, $-x+\frac{1}{2},y+\frac{1}{2},-z+\frac{1}{2}$; #10, $x-\frac{1}{2},-y+\frac{1}{2},z+\frac{1}{2}$; #11, $x+1,y,z$.
[b] Square brackets indicate bonds longer than 3 Å, not included in the bond-valence sums ($\sum s$) for Ag(2) and Ag(3).

NH_4^+ ions on the Ag^+ sites. Alternatively, the Ag deficiency in the β-$AgZnPO_4$ crystals could correspond to a slightly phosphorus-rich composition, $Ag_{0.82}Zn_{0.94}P_{1.06}O_4$, resulting from the substitution reaction $0.18Ag^+ + 0.06Zn^{2+} = 0.06P^{5+}$. However, no evidence of this substitution was found either in the electron microprobe analysis (yielding a P/Zn ratio of 1.00) or in the structural data (e.g., bond lengths in Table 7).

DESCRIPTION OF THE CRYSTAL STRUCTURES

The crystal structure of $AgBePO_4$ is shown in Fig. 1 and the corresponding bond lengths and angles are listed in Table 6. $AgBePO_4$ is isostructural with the mineral beryllonite, $NaBePO_4$ (15), with only a small increase in the unit cell volume (3.5%) due to the larger size of the Ag^+ cation. The corner-sharing BeO_4 and PO_4 tetrahedra form a fully ordered framework containing two types of rings with distinct topologies: one third are UDUDUD rings around the Ag(1) sites and two thirds are UUDUDD rings around the Ag(2) and Ag(3) sites (where U and D represent tetrahedra pointing up and down, respectively). All three Ag sites have irregular coordinations which are ninefold for Ag(1) and sixfold for Ag(2) and Ag(3), if only bonds shorter than 3 Å are included (cf. Table 6). The bond valences, however, indicate that the coordinations of the Ag(2) and Ag(3) sites are essentially tetrahedral and trigonal bipyramidal, respectively, with a number of weaker bonds that must be taken

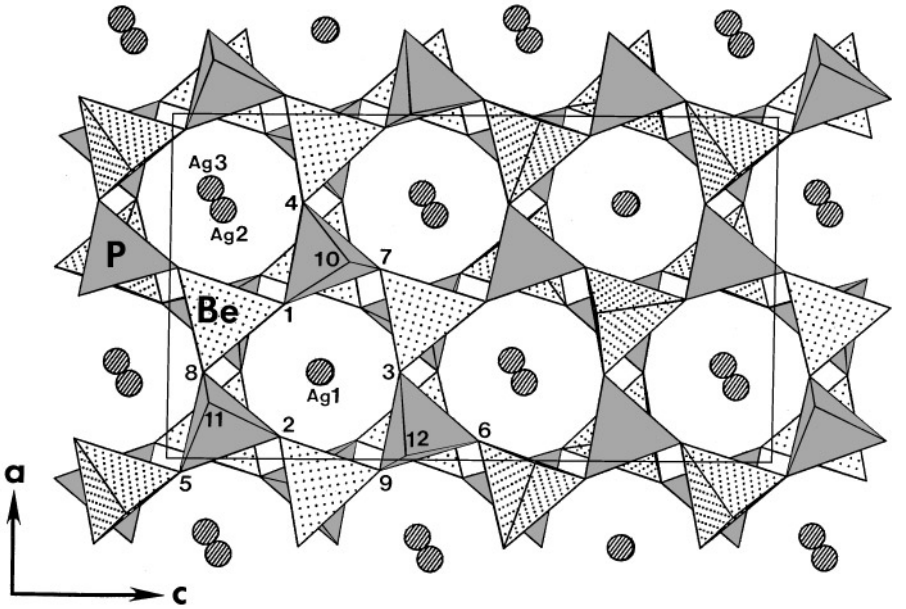

FIG. 1. View of the $AgBePO_4$ structure projected on the (010) plane of the monoclinic unit cell. The corner-sharing PO_4 (shaded) and BeO_4 (dotted) tetrahedra form a beryllonite-type framework containing two types of rings: UDUDUD around the Ag(1) positions and UUDDUD around the Ag(2) and Ag(3) positions (where U and D represent tetrahedra pointing up and down, respectively). The numbers correspond to the oxygen positions of Table 3.

into account to achieve proper bond-valence sums ($\sum s =$ 0.91–0.97). The nine-coordinated Ag(1) site shows a strong underbonding ($\sum s = 0.76$) which remains significant even when the coordination number is increased to 12 ($\sum s = 0.86$).

The crystal structure of β-$AgZnPO_4$ is shown in Fig. 2 and the corresponding bond lengths and angles are listed in Table 7. β-$AgZnPO_4$ is isostructural with $AgBePO_4$ with the same topology of the tetrahedral framework and with

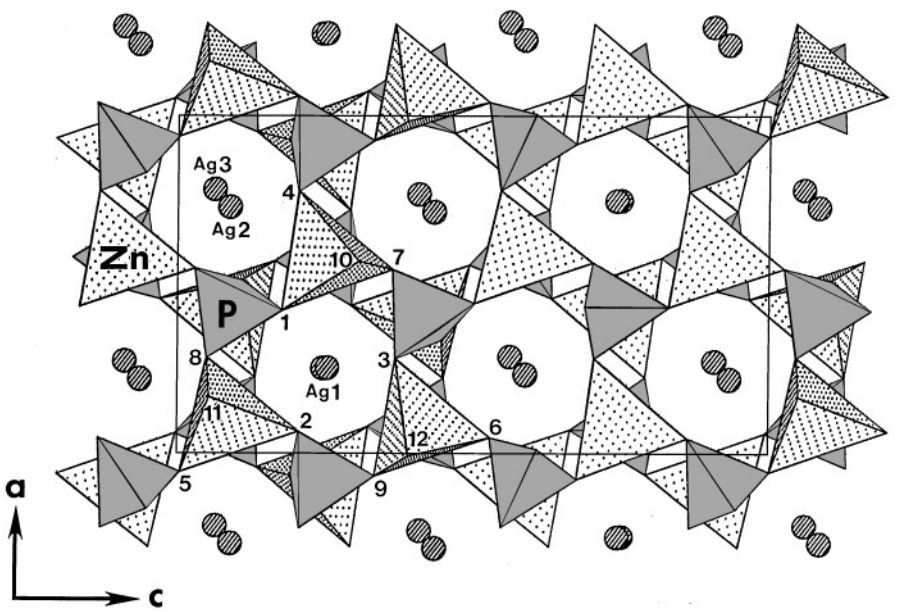

FIG. 2. View of the β-$AgZnPO_4$ structure projected on the (010) plane of the monoclinic unit cell. The corner-sharing PO_4 (shaded) and ZnO_4 (dotted) tetrahedra form the same beryllonite-type framework as in $AgBePO_4$ (cf. Fig. 1). The tetrahedral tilting is visibly more pronounced than in $AgBePO_4$ due to the larger difference between the Zn–O and P–O bond distances. The numbers correspond to the oxygen positions of Table 4.

TABLE 7
Bond Lengths (Å), Bond Valences (s), and Selected Bond Angles (°) in β-$AgZnPO_4$[a]

	l	s		
			P(2)–O(7)	1.530(2)
			P(2)–O(3)	1.530(2)
Ag(1)–O(2)#1	2.505(2)	0.151	P(2)–O(5)#10	1.535(2)
Ag(1)–O(3)#1	2.538(2)	0.138		
Ag(1)–O(1)#1	2.635(2)	0.106	P(3)–O(12)#1	1.526(2)
Ag(1)–O(2)	2.864(2)	0.057	P(3)–O(8)	1.531(2)
Ag(1)–O(1)	2.883(2)	0.054	P(3)–O(6)	1.533(2)
Ag(1)–O(10)#1	2.886(3)	0.054	P(3)–O(1)	1.534(2)
Ag(1)–O(3)	2.951(2)	0.045		
Ag(1)–O(12)#1	3.110(2)	0.029	Zn(1)–O(4)	1.919(2)
Ag(1)–O(11)#1	3.168(2)	0.025	Zn(1)–O(7)	1.930(2)
[Ag(1)–O(8)	3.309(2)	0.017][b]	Zn(1)–O(1)	1.939(2)
	$\sum s$	0.66	Zn(1)–O(10)	1.950(2)
Ag(2)–O(9)#3	2.351(2)	0.229	Zn(2)–O(11)	1.927(2)
Ag(2)–O(11)#4	2.376(2)	0.214	Zn(2)–O(8)	1.935(2)
Ag(2)–O(6)	2.473(2)	0.164	Zn(2)–O(2)	1.937(2)
Ag(2)–O(4)	2.498(2)	0.154	Zn(2)–O(5)#2	1.939(2)
Ag(2)–O(7)#3	2.527(2)	0.142		
Ag(2)–O(5)	3.078(2)	0.032	Zn(3)–O(6)#10	1.935(2)
[Ag(2)–O(1)	3.449(2)	0.012]	Zn(3)–O(9)#2	1.939(2)
	$\sum s$	0.93	Zn(3)–O(12)	1.944(2)
			Zn(3)–O(3)	1.947(2)
Ag(3)–O(8)#6	2.282(2)	0.275		
Ag(3)–O(10)#7	2.337(2)	0.237		
Ag(3)–O(5)	2.399(2)	0.201	P(3)–O(1)–Zn(1)	122.8(1)
Ag(3)–O(12)#1	2.481(2)	0.161	P(1)#2–O(2)–Zn(2)	118.8(1)
Ag(3)–O(6)	3.026(2)	0.037	P(2)–O(3)–Zn(3)	121.1(1)
Ag(3)–O(4)	3.048(2)	0.035	P(1)–O(4)–Zn(1)	129.9(1)
[Ag(3)–O(5)#8	3.215(2)	0.022]	P(2)#5–O(5)–Zn(2)#9	122.1(1)
[Ag(3)–O(7)#7	3.411(2)	0.013]	P(3)–O(6)–Zn(3)#5	121.0(1)
	$\sum s$	0.94	P(2)–O(7)–Zn(1)	121.6(1)
			P(3)–O(8)–Zn(2)	122.6(1)
P(1)–O(4)	1.518(2)		P(1)–O(9)–Zn(3)#9	123.1(1)
P(1)–O(9)	1.528(2)		P(1)#3–O(10)–Zn(1)	132.6(1)
P(1)–O(10)#7	1.528(2)		P(2)#11–O(11)–Zn(2)	131.5(1)
P(1)–O(2)#9	1.537(2)		P(3)#11–O(12)–Zn(3)	132.3(1)
P(2)–O(11)#1	1.528(2)			

[a] Symmetry transformations used to generate equivalent atoms: #1, $-x+\frac{1}{2},y-\frac{1}{2},-z+\frac{1}{2}$; #2, $x-1,y,z$; #3, $-x+\frac{3}{2},y+\frac{1}{2},-z+\frac{1}{2}$; #4, $-x+1,-y+1,-z$; #5, $x+\frac{1}{2},-y+\frac{1}{2},z-\frac{1}{2}$; #6, $-x+1,-y,-z$; #7, $-x+\frac{3}{2},y-\frac{1}{2},-z+\frac{1}{2}$; #8, $-x+2,-y,-z$; #9, $x+1,y,z$; #10, $x-\frac{1}{2},-y+\frac{1}{2},z+\frac{1}{2}$; #11, $-x+\frac{1}{2},y+\frac{1}{2},-z+\frac{1}{2}$.

[b] Square brackets indicate long bonds not included in the bond-valence sums ($\sum s$).

fully ordered, but interchanged, Zn and P positions (cf. Figs. 1 and 2). The significant increase in cell dimensions and cell volume (16%; cf. Table 1) is due to the Zn–O bonds being much longer than the Be–O bonds (about 1.93 Å and 1.63 Å, respectively). The larger cell volume in β-$AgZnPO_4$ requires a stronger degree of tilting within the tetrahedral framework in order to adjust its cavity size to the bonding requirements of the Ag^+ cations. This greater amount of framework distortion is revealed by the Zn–O–P angles, which are about 10° smaller than the Be–O–P angles, and also by the Ag coordination environments. This is particularly noticeable for the Ag(2) and Ag(3) sites, for which the bond lengths are actually slightly shorter in β-$AgZnPO_4$ and the pseudo-trigonal bipyramidal and tetrahedral coordinations are more apparent (cf. Tables 6 and 7). Bond-valence sums indicate that the nine-coordinated Ag(1) site remains even more underbonded in β-$AgZnPO_4$ ($\sum s = 0.66$) than in $AgBePO_4$ ($\sum s = 0.76$), and this strong underbonding appears to be the main reason for the instability of β-$AgZnPO_4$ at room temperature (see later).

The crystal structure of α-$AgZnPO_4$ is shown in Fig. 3 and the corresponding bond lengths and angles are listed in Table 8. Contrary to what had been previously proposed (22), the ordered tetrahedral framework does not have the same topology as the nepheline structure (containing UDUDUD rings only) but has, instead, a topology identical to those of high-T $NaCoPO_4$ (7, 8) and low-T/high-P $KZnPO_4$ (19) with two types of rings: one quarter of UDUDUD rings around the Ag(1) sites and three quarters of UUUDDD rings around the Ag(2) sites. Like the UUDDUD rings of the beryllonite structure, the unsymmetrical UUUDDD rings of the α-$AgZnPO_4$ structure allow an off-center displacement of the Ag^+ cations, yielding a pseudo-tetrahedral coordination around the Ag(2) sites. The Ag(2) environment is similar to that of the Ag(3) sites in β-$AgZnPO_4$ and bonds longer than 3 Å must also be taken

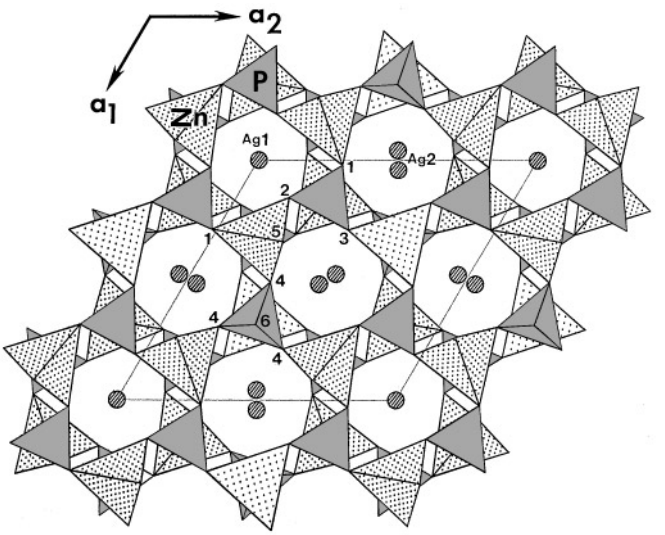

FIG. 3. View of the α-$AgZnPO_4$ structure projected on the (001) plane of the hexagonal unit cell. The framework of corner-sharing PO_4 (shaded) and ZnO_4 (dotted) tetrahedra has a different topology with UDUDUD rings around the Ag(1) positions and UUUDDD rings around the Ag(2) positions. The latter are strongly shifted off-center and achieve pseudotetrahedral coordination (cf. Table 8). The numbers correspond to the oxygen positions of Table 5; only one position is shown for the split O(6) atom.

TABLE 8
Bond Lengths (Å), Bond Valences (*s*), and Selected Bond Angles (°) in α-$AgZnPO_4$[a]

	l	*s*		
			Zn(2)–O(4)#15	1.921(2)
Ag(1)–O(2)#1	2.540(2) (×3)	0.137	Zn(2)–O(1)#2	1.942(2)
Ag(1)–O(2)	2.812(2) (×3)	0.066	Zn(2)–O(2)#1	1.943(2)
Ag(1)–O(5)#1	3.174(2) (×3)	0.025	Zn(2)–O(5)#22	1.947(2)
		$\sum s$ 0.68		
			P(1)–O(6)	1.511(4)
Ag(2)–O(5)#9	2.336(2)	0.238	P(1)–O(4)	1.537(2) (×3)
Ag(2)–O(4)#9	2.351(2)	0.229		
Ag(2)–O(1)#10	2.368(2)	0.218	P(2)–O(2)	1.530(2)
Ag(2)–O(3)#11	2.551(2)	0.133	P(2)–O(5)	1.533(2)
Ag(2)–O(3)#12	3.087(2)	0.031	P(2)–O(1)	1.536(2)
Ag(2)–O(4)#2	3.117(2)	0.029	P(2)–O(3)	1.537(2)
Ag(2)–O(6)#13	3.141(8)	0.027		
[Ag(2)–O(6)#16	3.381(14)	0.014][b]		
[Ag(2)–O(4)#10	3.426(2)	0.013]	P(2)–O(1)–Zn(2)#7	117.7(1)
		$\sum s$ 0.91	P(2)–O(2)–Zn(2)#8	124.1(1)
			P(2)–O(3)–Zn(1)#24	120.2(1)
			P(1)–O(4)–Zn(2)#24	121.1(1)
Zn(1)–O(6)	1.890(4)		P(2)–O(5)–Zn(2)#27	132.4(1)
Zn(1)–O(3)#1	1.939(2) (×3)		P(1)–O(6)–Zn(1)	165.8(4)

[a] Symmetry transformations used to generate equivalent atoms: #1, $x-y,x,z+\frac{1}{2}$; #7, $x-y,x,z-\frac{1}{2}$; #8, $y,-x+y,z-\frac{1}{2}$; #9, $x-y+1, x,z+\frac{1}{2}$; #10, $-x+y+1,-x+1,z$; #11, $-y+1,x-y,z$; #12, $y+1,-x+y+1,z+\frac{1}{2}$; #13, $x+1,y,z$ #15 $-x+1,-y+1,z+\frac{1}{2}$; #16, $-y+2,x-y+1,z$; #22, $x,y,z+1$; #24, $-x+1,-y+1,z-\frac{1}{2}$; #27, $x,y,z-1$.

[b] Square brackets indicate long bonds not included in the bond-valence sums ($\sum s$).

into account to achieve a proper bond-valence sum (cf. Table 8). Due to symmetry constraints, the ninefold coordination of the Ag(1) site in α-$AgZnPO_4$ is more regular but, as in β-$AgZnPO_4$, it also results in a strong underbonding ($\sum s = 0.68$). The Zn–O–P angles indicate a similar degree of distortion of the tetrahedral frameworks in α- and β-$AgZnPO_4$, except for the larger Zn–O(6)–P angle of 165.8° in the α-phase structure (cf. Table 8). The statistical splitting of the O(6) position around the threefold axis (about 0.3 Å from the axis; cf. Table 5) leads to unresolved structural disorder in α-$AgZnPO_4$, whereas a similar disorder is resolved by the formation of a $3\times c$ superstructure in $NaCoPO_4$ (7, 8), or an $a\times\sqrt{3}$ superstructure in $KZnPO_4$ (19). Electron diffraction showed no evidence of a superstructure in α-$AgZnPO_4$ and, in particular, the $2\times c$ superstructure reported previously (22) could not be observed either in the flux-grown single crystals or in the microcrystalline powder synthesized by solid-state reaction.

THE α–β TRANSFORMATION IN $AgZnPO_4$

From the descriptions of the α-$AgZnPO_4$ and β-$AgZnPO_4$ structures presented herein, it is clear that the α–β polymorphic transformation is first order and reconstructive in nature, involving a change in the topology of the [$ZnPO_4$] tetrahedral framework. The (high-*T*) β → (low-*T*) α transformation is therefore expected to be sluggish and, not surprisingly, was not observed during our DTA experiments using typical cooling rates of 10°C/min. Nevertheless, powder X-ray diffraction experiments using microcrystalline $AgZnPO_4$ powder have shown that the transformation is completely reversible and truly polymorphic in nature, without any detectable change in composition. Accordingly, the silver deficiency found in the β-$AgZnPO_4$ single crystals is believed to be purely accidental and was probably introduced after the crystal growth (vide supra).

The structure determinations confirm that the (quenched) high-*T* β-$AgZnPO_4$ phase adopts a monoclinic beryllonite-type structure similar to that of $NaZnPO_4$ (16) and show that the low-*T* α-$AgZnPO_4$ phase crystallizes with a hexagonal structure similar to that of high-*P*/low-*T* $KZnPO_4$ (17). This lowering of symmetry with increasing temperature is unusual, especially as it is accompanied by only a marginal change in volume (89.8 and 90.3 $Å^3$ per $AgZnPO_4$ formula unit for the α and quenched β phases, respectively —although, of course, the volume difference at the transition temperature may well be larger). From a crystal chemical viewpoint, the greater stability of the α-phase at room temperature can be understood in terms of the bonding environments of the Ag^+ cations. As shown by the bond-valence sums in Tables 7 and 8, the bonding environments in the α and β structures are satisfactory for all atoms, except for the Ag(1) sites, which are severely underbonded ($\sum s = 0.67$) in both structures. The coordinations around these sites are rather irregular (with three short bonds only) while the coordinations around the remaining sites have a more regular geometry (pseudotetrahedral for Ag(2) in α-$AgZnPO_4$ and Ag(3) in β-$AgZnPO_4$). Whereas the Ag(1) sites account for two thirds of the Ag atoms in the β-phase, they account for one quarter only in the α-phase so that, overall, the bonding of the Ag^+ cations improves during the β → α transformation. The comparison between the two beryllonite-type structures of β-$AgZnPO_4$ and $AgBePO_4$ also supports this interpretation of the phase transition in $AgZnPO_4$: no phase transformation has been observed for $AgBePO_4$ and, indeed, the bonding around all three Ag sites is satisfactory in the room-temperature structure (Σs = 0.86–0.92; cf. Table 6) as a result of the smaller cell dimensions due to the shorter Be–O bonds. As well, the distortion of the tetrahedral framework is significantly less pronounced in $AgBePO_4$ than in β-$AgZnPO_4$ (with mean $\langle T\text{–O–}T\rangle$ angles of 135 and 125°, respectively; cf. Tables 6 and 7), indicating that the [$BePO_4$] framework can accommodate the Ag^+ cations more easily at room temperature.

The relationship between the α and β phases of $AgZnPO_4$ was also investigated by preparing mixed phases involving the partial substitution of Ag^+ cations by smaller Na^+ and larger K^+ cations. The introduction of K^+ ions was found to destabilize the α-phase completely and only beryllonite-type β-$(Ag_{1-x}K_x)ZnPO_4$ solid solutions could be synthesized at 450°C, i.e., well below the transition temperature of

pure $AgZnPO_4$. As expected, the unit cell of the β-phase was observed to expand with its K content, resulting in a volume increase of 3.2% for $x = 0.3$. This expansion was also found to be highly anisotropic, with a 2.5% increase of the b-axis alone, probably resulting from the "opening" of the T–O–T angles at the O(10), O(11), and O(12) positions of the beryllonite-type [$ZnPO_4$] framework (cf. Fig. 2). The stability of these β-$(Ag_{1-x}K_x)ZnPO_4$ phases suggests that the larger K^+ ions occupy the Ag(1) positions which are severely underbonded in the unsubstituted β-$AgZnPO_4$ structure (vide supra). The substitution of Na^+ for Ag^+ was found to yield a narrow α-$(Ag_{1-x}Na_x)ZnPO_4$ solid solution limited to $x = 0.1$ for phases synthesized at 450°C. DSC measurements indicated that Na substitution also destabilized the α-$AgZnPO_4$ structure slightly, decreasing the temperature of the $\alpha \rightarrow \beta$ transition from 671°C for $AgZnPO_4$ to 619°C for $(Ag_{0.9}Na_{0.1})ZnPO_4$. This result is consistent with the stability of the beryllonite-type structure reported for $NaZnPO_4$ (18) but the latter has also been reported to undergo several uncharacterized phase transitions (29), including one at 390°C which could correspond to a transformation between a high-T beryllonite phase and a low-T phase isostructural with α-$AgZnPO_4$. Work is in progress to characterize the polymorphism of $NaZnPO_4$ in more detail.

ACKNOWLEDGMENTS

This work was supported by a research grant to J.B. from the Canadian Natural Sciences and Engineering Research Council. The single-crystal data were collected by Dr. J. Britten in the Chemistry Department of McMaster University. The electron microprobe analyses were done by Dr. C. Cermignani in the Department of Earth Sciences of the University of Toronto.

REFERENCES

1. F. Liebau, "Structural Chemistry of Silicates." Springer-Verlag, New York, 1985.
2. C. M. B. Henderson and D. Taylor, *Miner. Mag.* **45,** 111 (1982).
3. J. Barbier and M. E. Fleet, *Phys. Chem. Miner.* **16,** 276 (1988).
4. B. Liu and J. Barbier, *J. Solid State Chem.* **102,** 115 (1993).
5. M. Luján, F. Kubel, and H. Schmid, *Z. Naturforsch., B* **49,** 1256 (1994).
6. M. Luján, F. Kubel, and H. Schmid, *Z. Naturforsch., B* **50,** 1210 (1995).
7. R. Hammond and J. Barbier, *Acta Crystallogr., Sect. B* **52,** 440 (1996).
8. P. Feng, X. Bu, S. H. Tolbert, and G. D. Stucky, *J. Am. Chem. Soc.* **119,** 2497 (1997).
9. S. Y. Huang, R. von der Mühll, J. Ravez, and P. Hagenmuller, *Z. Kristallogr.* **209,** 118 (1994).
10. C. S. Liang, H. Eckert, T. E. Gier, and G. D. Stucky, *Chem. Mater.* **5,** 597 (1993).
11. M. Quarton, *Eur. J. Solid State Inorg. Chem.* **28,** 289 (1991).
12. S. H. M. Poort, W. P. Blokpoel, and G. Blasse, *Chem. Mater.* **7,** 1547 (1995).
13. G. Engel, *Neues Jb. Miner. Abh.* **127,** 197 (1976).
14. ICDD data base.
15. G. Giuseppetti and C. Tadini, *Tschermaks Mineral. Petrogr. Mitt.* **20,** 2 (1973).
16. R. Masse and A. Durif, *J. Solid State Chem.* **73,** 468 (1988).
17. G. Wallez, S. Jaulmes, A. Elfakir, and M. Quarton, *J. Phys. III* **4,** 1197 (1994).
18. L. Elammari, J. Durand, L. Cot, and B. Elouadi, *Z. Kristallogr.* **180,** 137 (1987).
19. M. Andratschke, K.-J. Range, H. Haase, and U. Klement, *Z. Naturforsch., B* **47,** 1249 (1992).
20. L. Elammari and B. Elouadi, *J. Chim. Phys.* **88,** 1969 (1991).
21. D. Blum, A. Durif, and M. T. Averbuch-Pouchot, *Ferroelectrics* **69,** 283 (1986).
22. M. Andratschke, *Z. Anorg. Allg. Chem.* **601,** 103 (1991).
23. M. Quarton, M.-T. Oumba, W. Freundlich, and A.-W. Kolsi, *Rev. Chim. Miner.* **21,** 311 (1984).
24. G. M. Sheldrick, SHELXTL-Plus Release 4.1, Siemens Analytical X-ray Instruments Inc., Madison, WI, (1991).
25. G. M. Sheldrick, SHELXL93: Program for the Refinement of Crystal Structures, University of Göttingen, Germany, 1993.
26. A. J. Perotta and J. V. Smith, *Mineral. Mag.* **35,** 588 (1965).
27. M. Gregorkiewitz, *Bull. Miner.* **107,** 499 (1984).
28. R. Hammond and J. Barbier, *Acta Crystallogr., Sect. B* **54,** 211 (1998).
29. B. Elouadi, L. Elammari, and J. Ravez, *Ferroelectrics* **56,** 17 (1984).